Clay Minerals (2022), **57**, 77–86
doi:10.1180/clm.2022.23

CAMBRIDGE UNIVERSITY PRESS

Article

Application of supported Cu–Ru catalysts for the removal of trace olefins in aromatics

Xiao Liang, Naiwang Liu*, Li Shi and Xuan Meng
East China University of Science and Technology, Shanghai 200237, China

Abstract

Exploring reliable hydrogenation catalysts to remove trace olefins in aromatic hydrocarbons through hydrogenation is an important topic. In this paper, a bimetallic Cu–Ru/montmorillonite (Cu–Ru/M) catalyst was prepared using a step-by-step impregnation method, and the effects of bimetallic catalysts on removing olefins were assessed. The catalysts were characterized using X-ray diffraction, Brunauer–Emmett–Teller specific surface area, inductively coupled plasma atomic emission spectrometry, high-resolution transmission electron microscopy and temperature-programmed reduction of H_2. The results show that there is a strong interaction between Cu and Ru on the Cu–Ru/M catalyst, which improves the dispersion of the metals on the surface of the support M. The hydrogen spillover phenomenon of Cu–Ru/M enhances its activity and adsorption capacity for hydrogen species. The catalytic performance test confirmed that the bimetallic catalyst has significantly greater activity and stability. The optimal loadings are 5% copper and 1% ruthenium, and the performance of this catalyst is comparable to those of noble-metal Pt/M catalysts.

Keywords: bimetal, hydrogenation, montmorillonite, olefins, synergy

(Received 6 November 2021; revised 14 May 2022; Associate Editor: Huaming Yang)

Aromatic compounds are important organic raw materials in the petrochemical industry. Aromatics include a variety of components, among which benzene, toluene and xylene (BTX) are considered first-class basic organic raw materials (Yao *et al.*, 2015; Zhao *et al.*, 2016; Liu *et al.*, 2017). At present, BTX are mainly obtained through naphtha-reforming and cracking processes. However, the aromatic products produced by these processes contain traces of olefin impurities, which affect product quality and even the safe operation of oil-distillation units; therefore, these traces must be removed. Traditional olefin removal methods include clay adsorption and hydrogenation removal. The white clay needs to be replaced frequently, which affects the environment negatively (Tian *et al.*, 2013). Hydrogenation catalysts can be divided into precious-metal catalysts and non-precious-metal catalysts. Among them, noble-metal catalysts represented by Pt and Pb have been proven to have high activity, stability and selectivity, but they are expensive and difficult to implement on a large scale. In contrast, non-precious metals represented by Cu and Ni are relatively inexpensive, but their activity and stability are significantly lower than those of precious-metal catalysts (Wang *et al.*, 2021). It is important, therefore, to explore and find high-efficiency and low-cost catalysts for hydrogenation and the removal of olefins to replace the precious-metal catalysts used in industry.

Cu has been shown to be a good hydrogenation metal, as it can be well-dispersed on a support surface and enhance the activity of hydrogenation catalysts (Álvarez-Rodríguez *et al.*, 2008; Kaźmierczak *et al.*, 2021; Zhang *et al.*, 2021b). Ru has also been shown to be a highly active and selective metal (Su *et al.*, 2007; Zheng *et al.*, 2021). Some studies have been conducted on the application of Cu–Ru bimetallic catalysts in hydrogenation reactions (Chen *et al.*, 2016; Lu *et al.*, 2017). Their use has been demonstrated in the synthesis of alcohols and lipids, the hydrogenolysis of glycerol, the catalytic wet oxidation of ammonia to nitrogen and even the hydrogenation of olefins with high activity and selectivity (Asedegbega-Nieto *et al.*, 2006; Chen *et al.*, 2016; Fu *et al.*, 2016; Soares *et al.*, 2016; Ban *et al.*, 2019). Compared with the C=O bond, it is beneficial thermodynamically to reduce the C=C bond instead (Asedegbega-Nieto *et al.*, 2006).

To explore the effects of bimetals on Cu–Ru/montmorillonite (Cu–Ru/M) catalysts for removing trace olefins from aromatic hydrocarbons, Cu–Ru bimetal catalysts were prepared using a step-by-step impregnation method with Cu and Ru as the active components and M as the support. We used Cu–Ru bimetallic catalysts to remove trace olefins from aromatic hydrocarbons *via* hydrogenation.

The catalytic mechanism of the bimetals was investigated using X-ray diffraction (XRD), N_2 isotherm adsorption–desorption, inductively coupled plasma atomic emission spectrometry (ICP-AES), high-resolution transmission electron microscopy (HR-TEM) and temperature-programmed reduction of H_2 (H_2-TPR). Due to the synergistic effects of bimetals, compared with the single metal Cu, the addition of Ru could increase significantly the dispersion of Cu on the support surface, provide more active sites and improve the activity of the catalyst through the strong interactions between the bimetals. Due to the hydrogen spillover effect, the addition of Ru could increase significantly the absorption and storage capacity of activated hydrogen on the surface of the Cu–Ru catalyst.

*Email: liunw@ecust.edu.cn
Cite this article: Liang X, Liu N, Shi L, Meng X (2022). Application of supported Cu–Ru catalysts for the removal of trace olefins in aromatics. *Clay Minerals* **57**, 77–86. https://doi.org/10.1180/clm.2022.23

Table 1. Components of the activated M.

Component	SiO_2	Al_2O_3	Fe_2O_3	CaO	MgO	K_2O	Na_2O	Other
Content (wt.%)	60.3	15.3	7.8	2.1	7.3	1.6	0.9	4.7

By assessing the catalytic activity at various loadings, it was determined that 5% Cu and 1% Ru were the optimal loadings. In the hydrogenation reaction, 5Cu–1Ru/M exhibits high activity and stability, even comparable to Pt-based catalysts, showing great potential for application in the field for removing trace olefins from aromatics. The focus of this research is to investigate the effects of the interactions between Cu and Ru on the hydrogenation catalysts and to develop high-performance Cu-based bimetallic catalysts.

Experimental

Materials

The activated M used in this study is produced in Zhejiang (China). The components of M are shown in Table 1. Cu $(NO_3)_2$•$3H_2O$ (analytical reagent) was purchased from Zhengzhou Chengchen Chemical Products Co., Ltd (China). $RuCl_3$•nH_2O (analytical reagent) was purchased from Shanghai Haohong Biomedical Technology Co., Ltd (China). Feed oil (hereinafter referred to as 'reforming oil') consisted of the mixed aromatics produced by the reforming unit of China Petrochemical Co., Ltd, Zhenhai Refinery Branch (China).

Catalyst preparation

The Cu-–Ru bimetallic catalyst was prepared using a two-step impregnation method. First, M was immersed in the solution of $Cu(NO_3)_2$•$3H_2O$ for 6 h, then dried at 110°C for 12 h. Second, the product from the first step was immersed in the $RuCl_3$•nH_2O solution for 3 h and dried at 110°C for 12 h. After calcination at 300°C for 4 h, we obtained the final catalyst, denoted as xCu–yRu/M, where x and y represent the mass percentages of Cu and Ru in this system (in elemental form). For example, 5Cu–1Ru/M indicates that Cu and Ru account for 5% and 1%, respectively, of the mass fraction of the whole catalyst (Cu + Ru + M). The additive amounts of M, $Cu(NO_3)_2$•$3H_2O$ and $RuCl_3$•nH_2O during the impregnation were 9.40, 1.90 and 0.25 g, respectively.

Catalyst characterization

The pore-structure parameters of the catalysts were obtained from N_2 isothermal adsorption–desorption experiments using an ASAP-2010 low-temperature N_2 adsorption–desorption instrument (Micromeritics, USA) with the pressure of N_2 set to 3 MPa. The sample mass for each experiment was ~0.10 g. Each sample was degassed in a vacuum at 200°C for 3 h to remove internal moisture, and then the adsorption measurement experiments were performed. After the adsorption and desorption process, we obtained the corresponding isotherm.

The grain size of a crystal was determined using XRD analysis. The main piece of equipment used was a D500 diffractometer (Siemens, Germany), with Cu-$K\alpha$ (40 kV, 100 mA) as the radiation source, and the scanning range was 3–80°2θ. An X-ray chamber reactor was used to register the spectra at high temperatures.

H_2-TPR was carried out using an Autochem 2910 (Micromeritics) instrument. Approximately 50 mg of catalyst powder, after pre-treatment (reaching 120°C at a rate of 10°C min^{-1} and maintaining this temperature for 1 h) to remove water and impurities, was exposed to a reducing gas consisting of 5.0 vol.% H_2 in Ar with a temperature ramp rate of 10°C min^{-1} from ambient temperature to 600°C.

The chemical compositions of the catalysts were determined using a 725-ES (Agilent, USA) ICP-AES instrument. The samples were dissolved completely in a suitable acid solution before analysis.

The morphologies of samples were observed using HR-TEM with a JEM-2100 apparatus (JEOL, Japan). A small amount of powder sample was placed on the Mo mesh, and TEM images were obtained using electron beams from an LaB6 filament (200 kV).

Catalytic reaction test

The reactor consisted of a 36 cm-long steel tube of dimensions 8.0 mm (outer diameter) × 1.5 mm (wall thickness of the reaction tube). The constant-temperature section was located in the middle part of the tube and was ~10 cm long; 1.3389 g of catalyst (screening 20–40 mesh) was loaded into the constant-temperature section of the reactor, and both ends were filled with quartz sand (20–40 mesh; Sinopharm Group Chemical Reagent Co., Ltd, China). The catalyst was first reduced at a H_2 flow rate of 50 mL min^{-1} and 300°C for 1 h. The hydrogenation reaction of the reforming oil was then carried out. The reaction temperature was 175°C and the pressure was 1.8 MPa. The volume flow rates of H_2 and the reforming oil were 18.0 and 0.9 mL min^{-1}, respectively; that is, the volume ratio of H_2 to reforming oil (VRHR) was 20. The ratio of reforming oil mass flow to catalyst mass (WHSV) was 35 h^{-1}.

An LC-6 Bromine Index Tester (Jiangsu Jiangyan Analytical Instrument Factory, China) was used to electrolyze KBr in an electrolyte to generate Br. A computer detected the electrical signal of the electrolytic KBr to obtain the degree of addition of unsaturated double bonds and then to obtain the bromine index of the aromatic hydrocarbon feedstock oil. We tested the bromine values of the raw oil and samples and then calculated the conversion rate of each sample. The conversion rate of olefin is $X = ((C_i - C_f)/C_i) \times 100\%$, where C_i is the initial olefin content and C_f is the final olefin content.

Gas chromatography (GC) was performed using a GC-1970 system (Tianmei Scientific Instrument Co., Ltd, China) to determine the composition of the reforming oil. The initial temperature was 60°C, which was then increased to 100°C at 10°C min^{-1} and maintained at that temperature for 2 min, and then further increased to 180°C at 10°C min^{-1} and maintained at that temperature for 4 min.

Results and discussion

N_2 adsorption–desorption isotherms

In the N_2 isothermal adsorption–desorption experiment, in the range where the relative partial pressure p/p_0 is low, the adsorption capacity increased rapidly with increasing relative partial pressure, as is shown in Figs 1 & 2. At higher p/p_0 values, a hysteresis loop can be observed. All catalysts showed typical type-IV isotherms and type-H3 loops based on the International Union of Pure and Applied Chemistry (IUPAC) classification, indicating the presence of mesopores.

https://doi.org/10.1180/clm.2022.23 Published online by Cambridge University Press

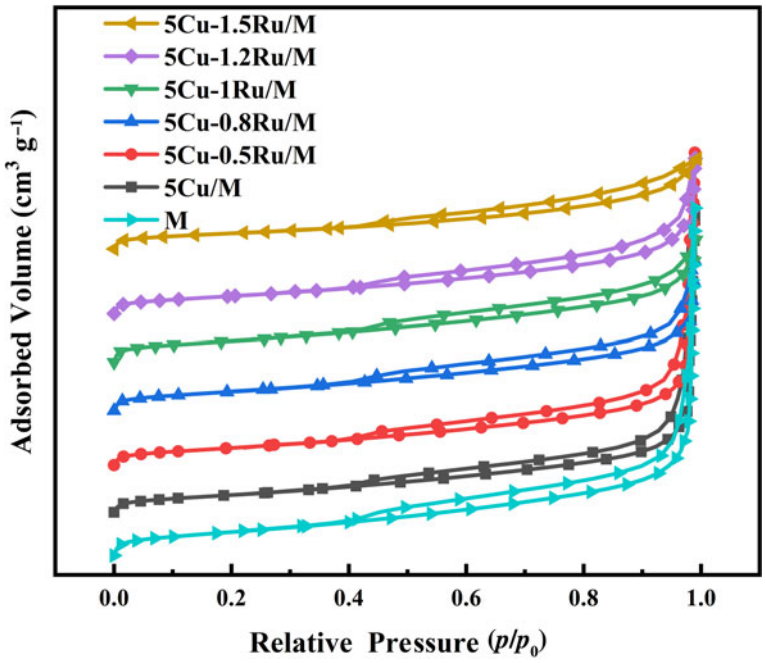

Fig. 1. N_2 adsorption–desorption isotherms of the catalysts with various Cu and Ru loadings.

Table 2 lists the Brunauer–Emmett–Teller specific surface area (S_{BET}), average total pore volume (V_{total}) and most probable pore diameter for the Barrett–Joyner–Halenda (BJH) adsorption of various catalysts. The S_{BET} first increased and then decreased with increasing Ru content, while V_{total} as measured using the BJH method showed the opposite trend.

It is worth noting that the addition of Ru increased the S_{BET} of the 5Cu/M catalyst. This may be due to the synergetic effect between Ru and Cu, which increases the dispersion of Cu on the surface of M (Ma *et al.*, 2019). In addition, Cu is more inclined to combine with Ru than M, thereby forming an alloy (Álvarez-Rodríguez *et al.*, 2008). These all lead to increased S_{BET}. However, S_{BET} did not always increase with increased Ru loading, as when the loading of Ru exceeded 1%, S_{BET} decreased. Previous research (Asedegbega-Nieto *et al.*, 2006) demonstrated that Cu and Ru tend to combine when loading is low, but when loading exceeds a certain value, Cu species separate from Ru and load onto the support M, which is consistent with our S_{BET} results. 5Cu–1Ru/M provides more sites for binding to active hydrogen species.

XRD characterization

XRD was performed to analyse the crystalline structure of the various catalysts, and the XRD traces are displayed in Fig. 3.

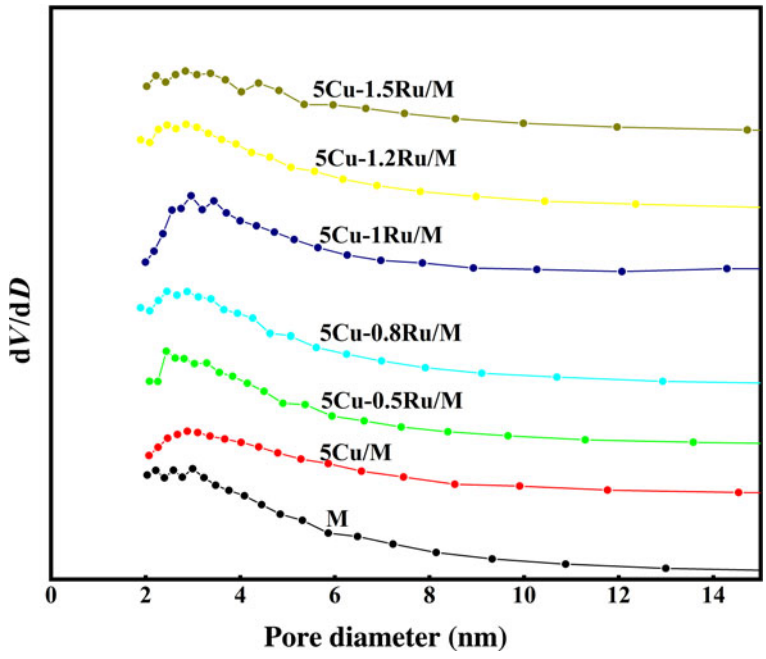

Fig. 2. Pore-size distribution curves of the various catalysts.

https://doi.org/10.1180/clm.2022.23 Published online by Cambridge University Press

Table 2. Structural parameters of the various catalysts.

Catalyst	S_{BET} (m^2 g^{-1})	V_{total} (cm^3 g^{-1})	PD (nm)
M	170	0.255	2.9
5Cu/M	106	0.947	2.9
5Cu–0.5Ru/M	122	0.851	3.0
5Cu–0.8Ru/M	129	0.825	2.9
5Cu–1Ru/M	140	0.332	2.5
5Cu–1.2Ru/M	120	0.424	3.0
5Cu–1.5Ru/M	117	0.436	3.1

For support M, typical structures of SiO_2 (JCPDF 46-1045) and M (JCPDF 13-0135) with lattice parameters of $a = 5.169$ Å, $b = 5.169$ Å and $c = 15.02$ Å could be observed. The characteristic peaks of SiO_2 and M remained essentially unchanged before and after modification. As such, it is shown that the structure of M is not destroyed during the preparation of the catalyst.

As is shown in Fig. 3, the characteristic diffraction peaks of Cu or Ru were not found. We attribute this to the light loading (up to 5%) of Cu and Ru (Stefanov *et al.*, 2015) and the synergistic effects of the bimetal, as the strong interaction between Cu and Ru can promote the dispersion of Cu and Ru (Ban *et al.*, 2019), making it difficult to observe the characteristic peaks of their related compounds.

H_2-TPR characterization

Figure 4a shows the H_2-TPR profiles of the catalysts. 1Ru/M had a reduction peak at ~179°C, which was much lower than the value for 5Cu/M, suggesting that the oxygen species in the 1Ru/M catalyst had relatively high reactivity. The 5Cu/M catalyst presented a main reduction peak at 296°C, and H_2 consumption continued up to a temperature of 440°C, indicating that Cu was harder to reduce than Ru. Note that there were three reduction peaks of 5Cu–1Ru/M at 151°C, 239°C and 280°C, which could be assigned to the hydrogen-consumption peak of Ru and the two hydrogen-consumption peaks of Cu (Asedegbega-Nieto *et al.*, 2006; Bulánek & Čičmanec, 2008). The hydrogen-consumption peaks of Ru and Cu in Cu–Ru/M all shifted to lower temperatures as a result of the hydrogen spillover effect (Stassi *et al.*, 2015). During the hydrogenation reaction, the active hydrogen species on Ru oxide surfaces would spill over to the nearby active metal Cu, changing from the original single active centre to the two Cu–Ru active centres (Zhang *et al.*, 2019), therefore making RuO_x and CuO_x easier to reduce with activated hydrogen species. There were two peaks for Cu, which could be assigned to the reduction of Cu^{2+} to Cu^+ and Cu^+ to Cu^0, respectively (Li *et al.*, 2013). This is also a typical manifestation of the hydrogen spillover effect in bimetallic catalysts (Stassi *et al.*, 2015). Due to the strong interaction between Cu and Ru, the two metals were bound tightly and the distribution was more dispersed (Soares *et al.*, 2016), which also resulted in a lower reduction temperature (Lu *et al.*, 2017).

The reducible behaviour of 5Cu–*y*Ru/M ($y = 0.5$, 0.8, 1.0, 1.2 or 1.5) was then investigated using H_2-TPR, and the results of this are shown in Fig. 4b. Except for 5Cu–1.5Ru/M, the shapes of the hydrogen-consumption peaks of the various 5Cu–*y*Ru/M catalysts were approximately the same. Note that there were two hydrogen-consumption peaks of Ru species in 5Cu–1.5Ru/M, which could be assigned to the Ru clusters that result from the separation of Ru species (>1%) from Cu species and Ru species that combined with Cu species (Fu *et al.*, 2016). With increasing Ru loading, the reduction temperature first decreased, as the reduction temperature for 5Cu–1Ru/M was less than that for 5Cu–0.5Ru/M by ~20°C, but when the Ru loading exceeded 1%, the reduction temperature increased gradually and shifted back towards its previous value. These results further support the notion of a strong interaction between Cu and Ru and the separation of Ru from the Cu surface when the Ru content was increased to >1%.

Integrating the H_2-TPR curves was performed to obtain the total hydrogen consumptions of the catalysts, and the results are shown in Table 3. By comparing the peak area of the hydrogen-consumption curve, it can be concluded that the addition of Ru not only improved the reduction activity of H species on the 5Cu/M catalyst, but also increased the adsorption capacity for H species (Álvarez-Rodríguez *et al.*, 2008; Huang *et al.*, 2021). Note that 5Cu–1Ru/M had the strongest reducibility and provided the most activation sites, which is consistent with the S_{BET} results and the H_2-TPR profiles.

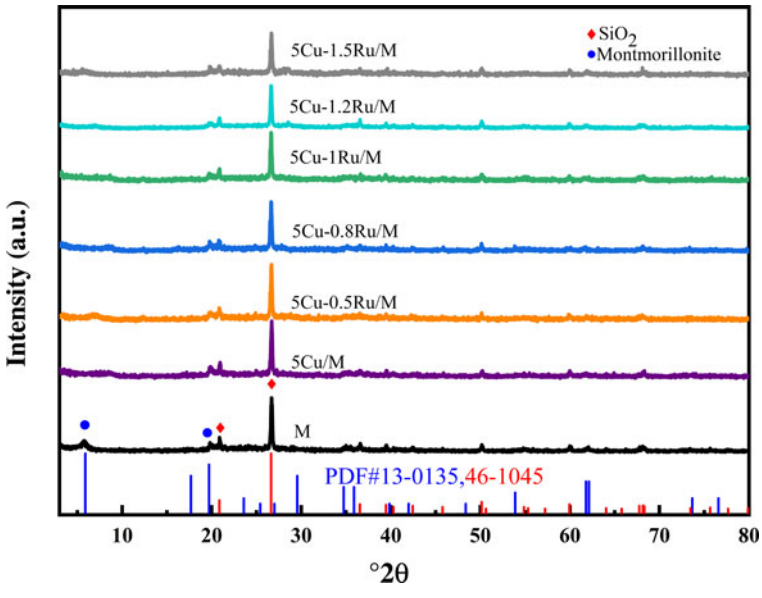

Fig. 3. XRD traces of the various catalysts.

https://doi.org/10.1180/clm.2022.23 Published online by Cambridge University Press

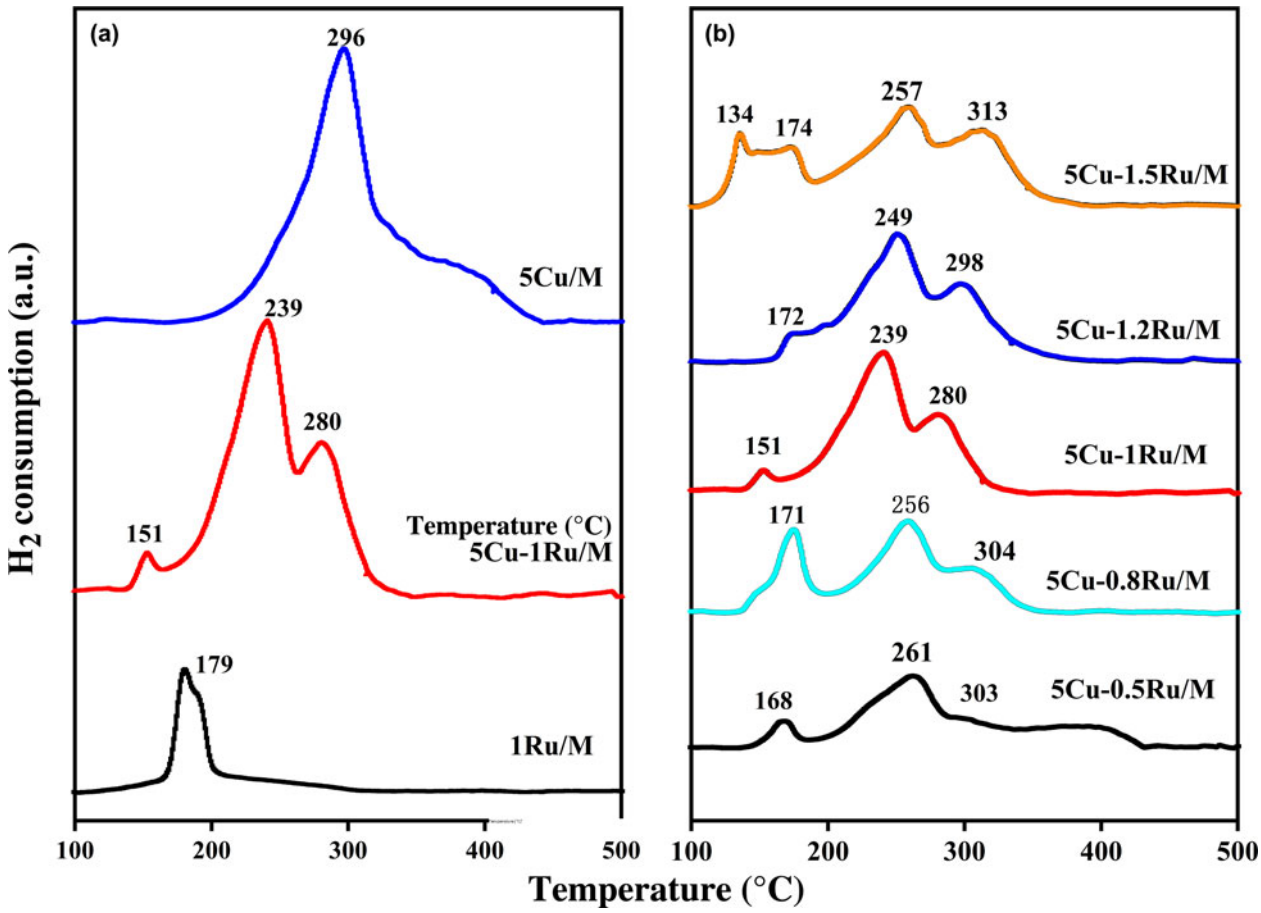

Fig. 4. H_2-TPR profiles of the non-reduced samples. (a) Comparison of Cu-based, Ru-based catalysts and Cu–Ru bimetallic catalysts. (b) Comparison of 5Cu–*y*Ru/M catalysts (y = 0.5, 0.8, 1.0, 1.2 or 1.5).

Inductively coupled plasma atomic emission spectrometry

To prove that Cu and Ru were loaded successfully on the M, the actual metal contents of the 5Cu–1Ru/M catalysts were determined using ICP-AES. The ICP-AES data show that the Cu content was 4.55 mg L^{-1}, while the Ru content was 0.96 mg L^{-1}. According to these calculations, for the 5Cu–1Ru/M catalyst, the actual loading of Cu was 4.55 wt.% and of Ru was 0.96 wt.%. Excluding instrument error and losses during the roasting process, these values are close to the theoretical loadings, proving that Cu and Ru can combine effectively with support M.

High-resolution transmission electron microscopy

HR-TEM images of M and 5Cu–1Ru/M are shown in Fig. 5. Figure 5a shows that M has a layered structure, which is consistent with the results from the N_2 adsorption–desorption isotherm experiments. The dispersion of metal oxides on the support was also studied using HR-TEM. Figure 5b shows that metal oxides were observed on the support surface. The metal-oxide particles are displayed in Fig. 5b as black dots, and the light grey region is the support, indicating that metal oxides were supported successfully on the surface of M. Most of the metal oxides were well dispersed, and only a few were agglomerated.

Table 3. Total hydrogen consumption of the various catalysts in H_2-TPR.

5Cu/M	5Cu–0.5Ru/M	5Cu–0.8Ru/M	5Cu–1Ru/M	5Cu–1.2Ru/M	5Cu–1.5Ru/M
8131	8814	9307	13,721	12,379	11,652

Comparison of the activity levels of the various catalysts

In the absence of hydrogenation, M also removes olefins *via* adsorption. To test its effect on olefin removal, we tested the activities of M and 5Cu–1Ru/M without hydrogenation, while the other reaction conditions were the same as with hydrogenation. The comparison of the conversion rates for removing olefins is shown in Fig. 6. M and 5Cu–1Ru/M removed very few olefins *via* adsorption, and so this process had a negligible effect on the results. Therefore, the catalysts mainly removed the olefins in the reforming oil *via* the hydrogenation reaction.

For the same catalysts, reagent diffusion is affected by particle size. To exclude the influence of reagent diffusion in these reaction conditions, we prepared 5–10, 20–40, 40–60 and 60–80 mesh 5Cu–1Ru/M catalysts and tested their performance under the same reaction conditions. The results are shown in Fig. 7. It can be observed that the conversion of the 5–10 mesh catalyst was significantly less than those of the 20–40, 40–60 and 60–80 mesh catalysts. However, there were no significant differences in conversion rates between the other catalysts, so for the 20–40 mesh catalysts the influence of reagent diffusion can be excluded in these reaction conditions.

https://doi.org/10.1180/clm.2022.23 Published online by Cambridge University Press

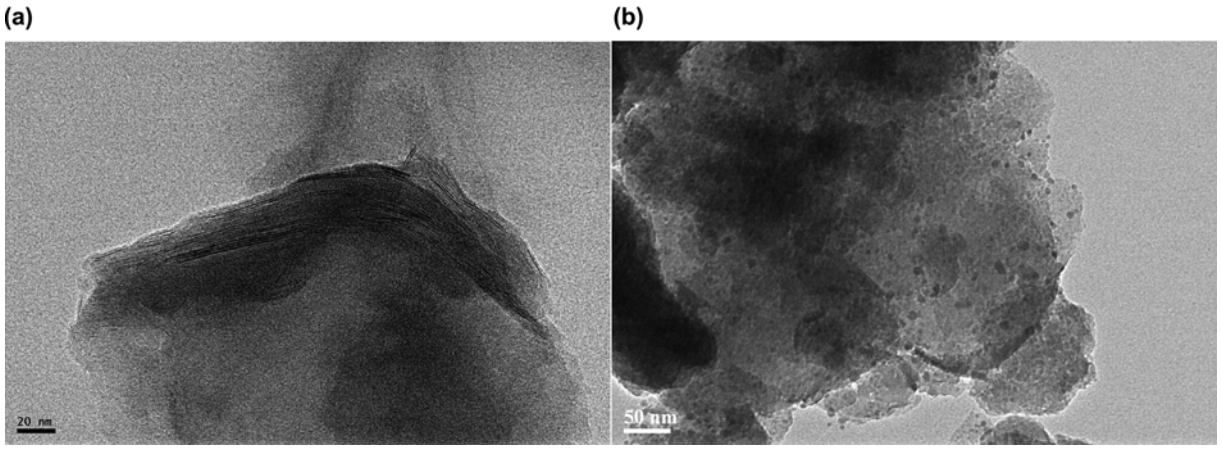

Fig. 5. HR-TEM images of (a) M and (b) 5Cu–1Ru/M.

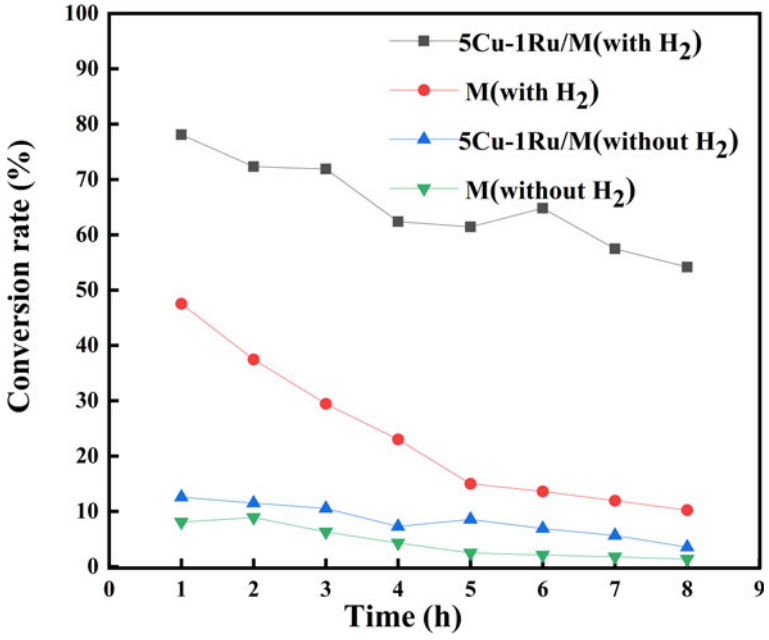

Fig. 6. Comparison of olefin-removal conversion of the catalysts with and without hydrogenation (WHSV = 35 h^{-1}, T = 175°C, P = 1.8 MPa, VRHR = 20).

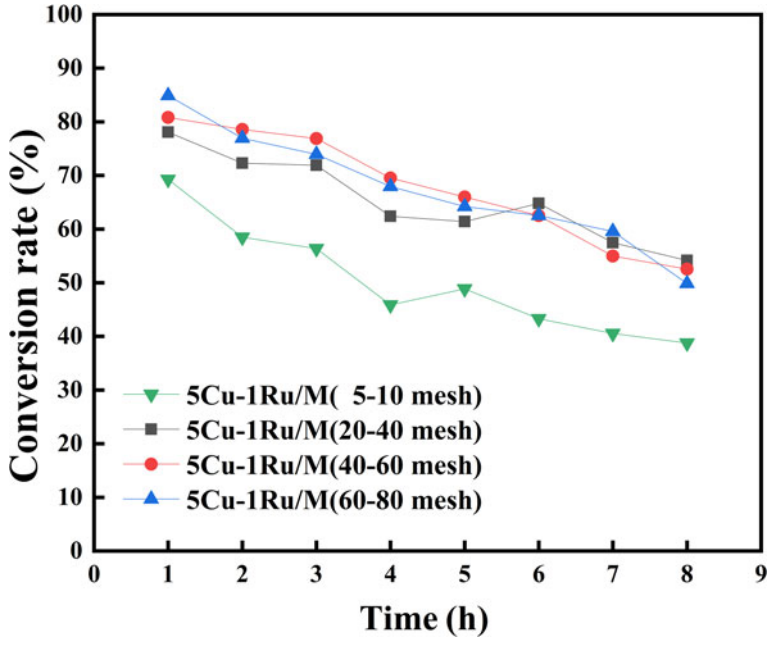

Fig. 7. Conversion of 5Cu–1Ru/M with various mesh numbers (WHSV = 35 h^{-1}, T = 175°C, P = 1.8 MPa, VRHR = 20).

https://doi.org/10.1180/clm.2022.23 Published online by Cambridge University Press

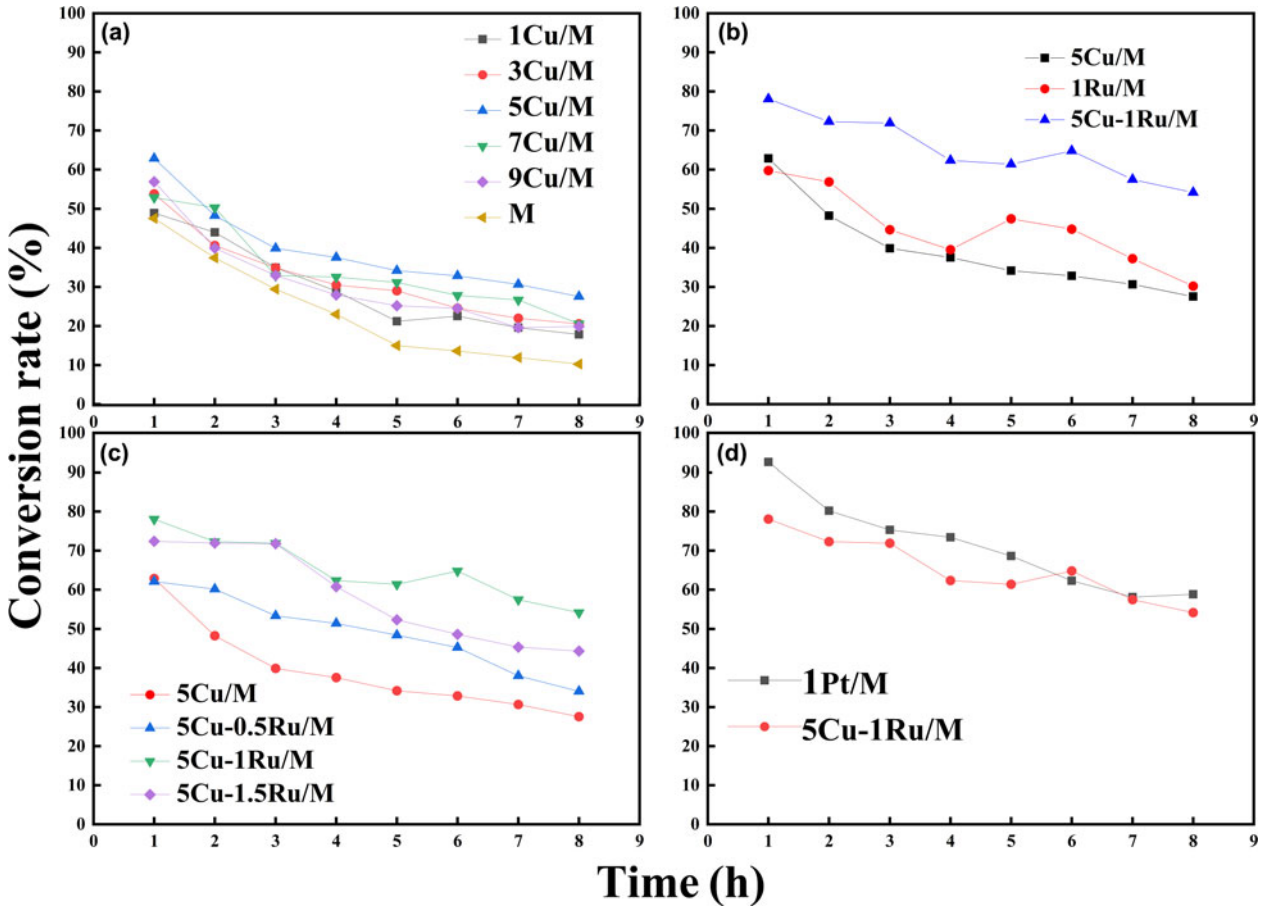

Fig. 8. Catalytic activity tests. (a) Comparison of Cu-based catalysts (WHSV = 35 h^{-1}, VRHR = 20). (b) Comparison of 5Cu/M, 1Ru/M and 5Cu–1Ru/M (WHSV = 35 h^{-1}, VHRH = 20). (c) Comparison of 5Cu–*y*Ru/M (*y* = 0.5, 1.0 or 1.5; WHSV = 35 h^{-1}, VRHR = 20). (d) Comparison of 5Cu–1Ru/M and 1Pt/M (WHSV = 35 h^{-1}, VRHR = 20).

Figure 8 shows the conversion rates of the various catalysts over time. As is shown in Fig. 8a, pure M could adsorb olefins, and it had the lowest activity and the worst stability. As Cu was loaded on M, the activity of the catalyst increased and the deactivation rate also reduced, demonstrating that Cu provided the active centre and improved the stability of the catalyst to a certain extent, confirming the good performance of Cu as the active metal in hydrogenation catalysts (Schittkowski *et al.*, 2017).

On this basis, by changing the loading of Cu, various *x*Cu/M (*x* = 1, 3, 5, 7 or 9) catalysts were prepared to compare their activities. It was found that 5Cu/M demonstrated greater activity than the other catalysts at the beginning of the reaction. Furthermore, in terms of application time of the catalysts, we compared the stability of their activity after 5 h of evaluation. As the loading of Cu increased, the activity of *x*Cu/M first increased and then decreased, and 5Cu/M performed best. This could be due to low levels of Cu being insufficient to increase the active sites for the hydrogenation reaction, while high levels of Cu would block the layered structure of the support M, which could be confirmed from the N_2 adsorption–desorption isotherm results. A 1Ru/M catalyst was also prepared. 1Ru/M performed well at 1 h, but then its performance began to decline sharply and finally stabilized at a similar value as that for 5Cu/M. Therefore, the single Cu or Ru metal catalysts were not suitable for catalytic hydrogenation. By contrast, the activity and stability of the 5Cu–1Ru/M catalyst were improved significantly. Due to the synergistic effects in bicomponent Cu–Ru/M catalysts, the addition of Ru could increase the dispersion and structural stability of Cu on the surface of the support, thus improving activity while slowing down the deactivation rate of the catalyst (Lu *et al.*, 2017). Moreover, due to the hydrogen spillover effect, the combined action of the bimetals added new active centres, and the activated hydrogen species reacted on the three active centres of Cu, Ru and support M at the same time, which increased the reaction rate significantly (Zhang *et al.*, 2019).

On this basis, the influence of various Ru loadings on Cu-based catalysts was explored. As is shown in Fig. 8c, we found that with increased Ru loading, the activity of 5Cu–*y*Ru/M (*y* = 0.5, 1.0 or 1.5) first increased and then decreased. Among these catalysts, 5Cu–1Ru/M demonstrated the greatest activity and stability, which is consistent with the N_2 adsorption–desorption isotherm results, confirming the greatest metal dispersibility for 5Cu–1Ru/M, which provided the greatest number of active sites to bind with active hydrogen species. Moreover, *via* H_2-TPR, 5Cu–1Ru/M was also shown to absorb and utilize the most active hydrogen species (Zhang *et al.*, 2019). Overall, we have verified through experiments that 5% Cu and 1% Ru are the optimal loadings for *x*Cu–*y*Ru/M catalysts.

Pt has been recognized as an excellent active metal for hydrogenation catalysts and has been used widely in industrial applications. Under the same reaction conditions, we compared the performance of 5Cu–1Ru/M with 1Pt/M catalysts. The Pt catalyst had extremely high activity (92%) at the beginning of the reaction, but this decreased rapidly over time, and the activity of the

https://doi.org/10.1180/clm.2022.23 Published online by Cambridge University Press

Table 4. Comparison of 5Cu–1Ru/M and Cu–Zn catalyst performance.

Catalyst	Conversation rate (8 h)
5Cu–1Ru/M	56%
Cu-Zn catalyst	47%

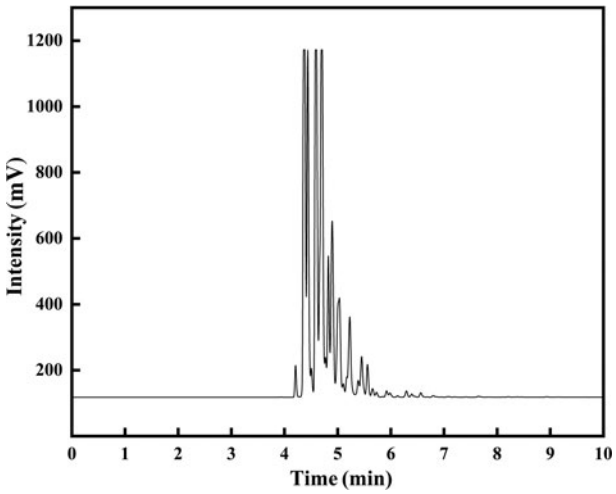

Fig. 9. Gas chromatogram of the reforming oil.

5Cu–1Ru/M catalyst was very close to that of the 1Pt/M catalyst after 6 h. Considering the high cost of Pt, this result is very satisfactory. In general, 5Cu–1Ru/M was comparable to the precious-metal Pt catalyst, showing great potential for replacing traditional noble-metal catalysts in the future.

In addition, we compared this catalyst with a Cu–Zn bimetallic hydrogenation catalyst (Wang *et al.*, 2021). The results of this are shown in Table 4. The two catalysts reacted at the same temperature, pressure and WHSV. However, the VRHR of the Cu–Zn catalyst was 250, while the VRHR for 5Cu–1Ru/M was 50. This also illustrates the excellent performance of 5Cu–1Ru/M.

The side-reactions during the experiment included mainly aromatic cracking and hydrogenation of benzene rings in aromatic molecules. We used GC to study the loss of aromatics in the reforming oil under these reaction conditions. The raw oil in this experiment was taken from the reformer of the refinery. Its composition is very complicated, as is shown in Fig. 9. To study the influence of side-reactions more clearly, we prepared a simulated oil. The simulated oil was prepared with *n*-heptane and mixed xylene, and the mass fraction of mixed xylene was 50%, which was selected to simulate the specific gravity of xylene in the feedstock oil. The simulated oil was hydrogenated catalytically under the same reaction conditions as the previous experiments, and the results of this are shown in Fig. 10. There was no GC of the sample after the reaction, which means that there was no aromatic cracking and hydrogenation of benzene rings in the aromatics. This occurred firstly because these side-reactions required severe conditions of high temperature and high pressure, which were not available in this hydrogenation experiment, and secondly because the catalyst had the effect of selective hydrogenation and the reaction process was relatively mild.

Mechanism of the hydrogenation process on the catalyst surface

It is believed generally that the olefin hydrogenation reaction takes place on the surface of a catalyst. Its mechanism is shown in Fig. 11. First, hydrogen is adsorbed on the huge surface of the

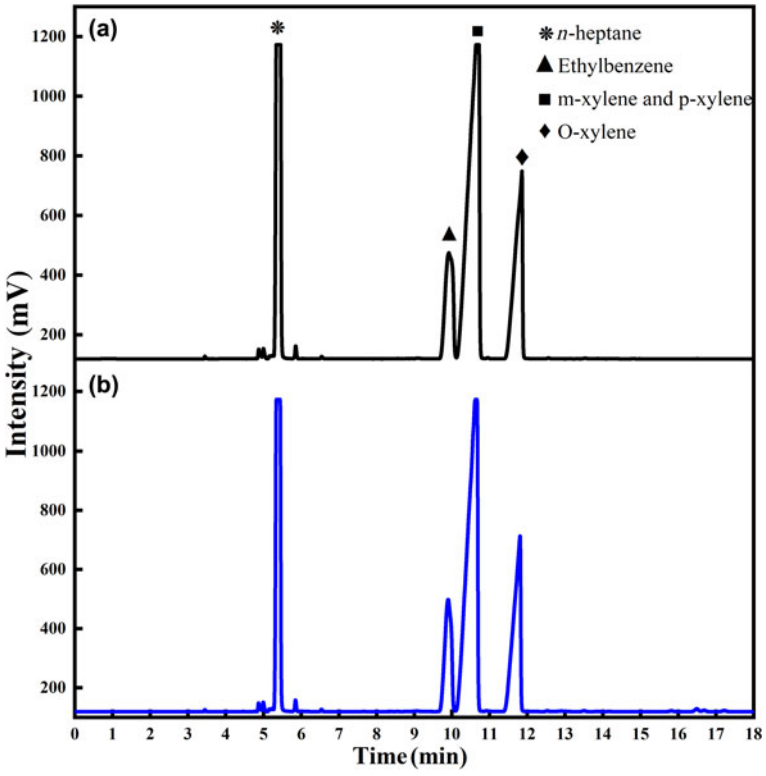

Fig. 10. Gas chromatograms of the simulated oil (a) before and (b) after reaction.

https://doi.org/10.1180/clm.2022.23 Published online by Cambridge University Press

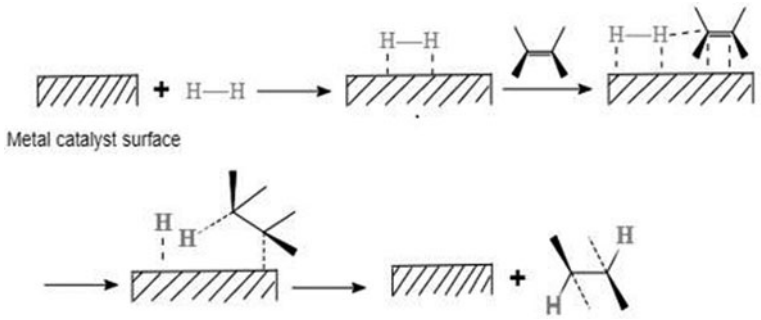

Fig. 11. The hydrogenation mechanism of olefins on a metal catalyst surface.

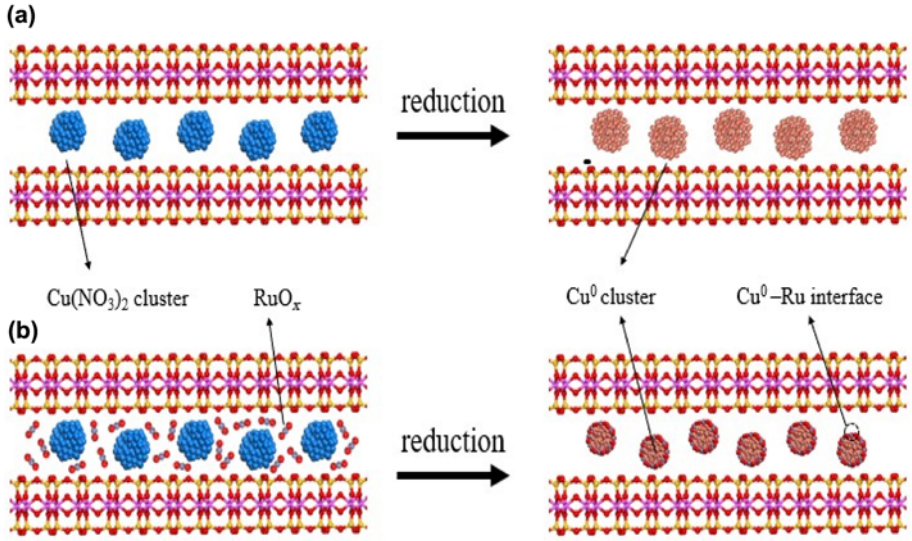

Fig. 12. The formation process of the catalyst surface.

finely dispersed metal, and the catalyst surface breaks the H–H covalent bond of hydrogen molecules, forming active hydrogen atoms. Second, at the same time, the olefin and the catalyst form a complex, and the π bond in the olefin is also weakened, which reduces greatly the activation energy required for the hydrogenation reaction and increases the reaction rate. Third, hydrogen atoms combine with the carbon atoms of the olefin double bond to form alkanes. As the adsorption capacity of the catalyst surface for alkanes is less than that for alkenes, the resulting alkanes dissociate from the catalyst surface. When alkanes are generated, the greater the number of active sites on the catalyst surface, the greater the number of olefins and hydrogen molecules that can be adsorbed at the same time, thereby accelerating the hydrogenation reaction rate. Excess metal will agglomerate and block the pore structure even more, which will cause a sharp decrease in the number of active sites (Wang *et al.*, 2021). This is consistent with our N_2 adsorption–desorption isotherm results. Moreover, the number of active sites is not the only factor that affects the reaction rate. The adsorption and desorption rate of active hydrogen and olefins on the surface and the adsorption capacity of the catalyst surface are also very significant factors (Centi & Perathoner, 1995).

The formation process of the catalyst surface is shown in Fig. 12. For single-metal Cu catalysts, after high-temperature calcination and reduction processes, Cu species converge into copper clusters, which will result in a reduction in the number of active sites. By contrast, in the Cu–Ru bimetallic catalyst, there is an interface effect between the two metals (Zhu *et al.*, 2021). A Cu–Ru interface is formed after calcination and reduction, and Ru species tend to combine with Cu species (Poels & Brands, 2000; Zhang *et al.*, 2021a), which improves the dispersion of Cu species greatly and also reduces the number and size of copper clusters (Zheng *et al.*, 2012). As a result, the adsorption and desorption rate and capacity for hydrogen on the surface of the catalyst are also improved significantly.

Conclusion

Cu–Ru/M bimetallic catalysts were prepared and characterized. Based on the 'Results and discussion' section, the following conclusions can be drawn:

(1) Cu and Ru can be loaded successfully onto M using a step-by-step impregnation method without changing the layered structure of M.
(2) There is an interaction between Cu and Ru, and appropriate loadings of Ru can increase the dispersion of Cu on the catalyst surface (Zhuang *et al.*, 2019).
(3) Due to the hydrogen spillover effect, the reducing ability of the Cu–Ru/M catalysts increases and more active hydrogen species can be adsorbed; 5Cu–1Ru/M had the strongest reducing ability.
(4) The optimal loadings of Cu–Ru/M bimetallic catalysts are 5% Cu and 1% Ru. 5Cu–1Ru/M shows excellent catalytic

https://doi.org/10.1180/clm.2022.23 Published online by Cambridge University Press

performance that is comparable to those of noble-metal Pt catalysts. 5Cu–1Ru/M did not lead to the loss of aromatics under these experimental conditions.

To further improve the performance of this catalyst, we will improve the preparation method and find better co-catalysts in the future.

References

Álvarez-Rodríguez J., Guerrero-Ruiz A., Rodríguez-Ramos I. & Arcoya A. (2008) Changes in the selective hydrogenation of citral induced by copper addition to Ru/KL catalysts. *Microporous and Mesoporous Materials*, **110**, 186–196.

Asedegbega-Nieto E., Bachiller-Baeza B., Guerrero-Ruíz A. & Rodríguez-Ramos I. (2006) Modification of catalytic properties over carbon supported Ru–Cu and Ni–Cu bimetallics. *Applied Catalysis A: General*, **300**, 120–129.

Ban C., Yang S., Kim H. & Kim D.H. (2019) Effect of Cu addition to carbon-supported Ru catalysts on hydrogenation of alginic acid into sugar alcohols. *Applied Catalysis A: General*, **578**, 98–104.

Centi G. & Perathoner S. (1995) Adsorption and reactivity of no on copper-on-alumina catalysts: II. Adsorbed species and competitive pathways in the reaction of no with NH_3 and O_2. *Journal of Catalysis*, **152**, 93v102.

Chen Y., Yu Z., Chen Z., Shen R., Wang Y., Cao X. *et al.* (2016) Controlled one-pot synthesis of RuCu nanocages and Cu@Ru nanocrystals for the regioselective hydrogenation of quinoline. *Nano Research*, **9**, 2632–2640.

Fu J., Yang K., Ma C., Zhang N., Gai H., Zheng J. & Chen B.H. (2016) Bimetallic Ru–Cu as a highly active, selective and stable catalyst for catalytic wet oxidation of aqueous ammonia to nitrogen. *Applied Catalysis B: Environmental*, **184**, 216–222.

Huang X., Liu Y., Wen H., Shen R., Mehdi S., Wu X. *et al.* (2021) Ensemble-boosting effect of Ru–Cu alloy on catalytic activity towards hydrogen evolution in ammonia borane hydrolysis. *Applied Catalysis B: Environmental*, **287**, 119960.

Kaźmierczak K., Salisu A., Pinel C., Besson M., Michel C. & Perret N. (2021) Activity of heterogeneous supported Cu and Ru catalysts in acceptor-less alcohol dehydrogenation. *Catalysis Communications*, **148**, 106179.

Li J., Wilken N., Kamasamudram K., Currier N.W., Olsson L. & Yezerets A. (2013) Characterization of active species in Cu–beta zeolite by temperature-programmed reduction mass spectrometry (TPR-MS). *Topics in Catalysis*, **56**, 201–204.

Liu J., Liu N., Ren K., Shi L. & Meng X. (2017) Sulfated zirconia synthesized in a one step solvent-free method for removal of olefins from aromatics. *Industrial & Engineering Chemistry Research*, **56**, 7693–7699.

Lu F., Yu C., Meng X., Chen G. & Zhao P. (2017) Degradation of highly concentrated organic compounds over a supported Ru–Cu bimetallic catalyst. *New Journal of Chemistry*, **41**, 3280–3289.

Ma Y.J., Cai Y.P., Wang G.J., Cui M.J., Sun C., Cao Z.H. & Meng X.K. (2019) Enhanced thermal stability by heterogeneous interface and columnar grain in nanoscale Cu/Ru multilayers. *Materials Science and Engineering: A*, **742**, 751–759.

Poels E.K. & Brands D.S. (2000) Modification of $Cu/ZnO/SiO_2$ catalysts by high temperature reduction. *Applied Catalysis A: General*, **191**, 83–96.

Schittkowski J., Tölle K., Anke S., Stürmer S. & Muhler M. (2017) On the bifunctional nature of Cu/ZrO_2 catalysts applied in the hydrogenation of ethyl acetate. *Journal of Catalysis*, **352**, 120–129.

Soares A.V.H., Salazar J.B., Falcone D.D., Vasconcellos F.A., Davis R.J. & Passos F.B. (2016) A study of glycerol hydrogenolysis over $Ru–Cu/Al_2O_3$ and $Ru–Cu/ZrO_2$ catalysts. *Journal of Molecular Catalysis A: Chemical*, **415**, 27–36.

Stassi J.P., Zgolicz P.D., Rodriguez V.I., de Miguel S.R. & Scelza O.A. (2015) Ga and In promoters in bimetallic Pt based catalysts to improve the performance in the selective hydrogenation of citral. *Applied Catalysis A: General*, **497**, 58–71.

Stefanov P., Todorova S., Naydenov A., Tzaneva B., Kolev H., Atanasova G. *et al.* (2015) On the development of active and stable $Pd–Co/\gamma\text{-}Al_2O_3$ catalyst for complete oxidation of methane. *Chemical Engineering Journal*, **266**, 329–338.

Su F.B., Lee F.Y., Lv L., Liu J.J., Tian X.N. & Zhao X.S. (2007) Sandwiched ruthenium/carbon nanostructures for highly active heterogeneous hydrogenation. *Advanced Functional Materials*, **17**, 1926–1931.

Tian Y., Meng X. & Shi L. (2013) Synthesis of SO_3H-functionalized ionic liquids and their novel application in removal of trace olefins from aromatics. *Industrial & Engineering Chemistry Research*, **52**, 6655–6661.

Wang L., Meng X., Wang S., Shi L., Hu X. & Liu N. (2021) Research and application of a non-noble metal catalyst in the removal of trace olefins from aromatics. *New Journal of Chemistry*, **45**, 3901–3908.

Yao J., Liu N., Shi L. & Wang X. (2015) Sulfated zirconia as a novel and recyclable catalyst for removal of olefins from aromatics. *Catalysis Communications*, **66**, 126–129.

Zhang X., Li H.-R., Zhao F.-G., Cui X.-Y., Ye F. & He L.-N. (2021b) Green process for hydrogenation of methyl ricinoleate to methyl 12-hydroxystearate over diatomite supported Cu/Ni bimetallic catalyst. *Green Chemical Engineering*, **2**, 187–196.

Zhang J., Gao Z., Wang S., Wang G., Gao X., Zhang B. *et al.* (2019) Origin of synergistic effects in bicomponent cobalt oxide-platinum catalysts for selective hydrogenation reaction. *Nature Communications*, **10**, 4166.

Zhang A., Wu S., Li Y., Zhang Q., Hu Q., Wu J. *et al.* (2021a) A novel synergetic effect between Ru and Cu nanoparticles for $Ru–Cu/Al_2O_3$ causes highly efficient photothermocatalytic Co_2 reduction with good durability. *Applied Surface Science*, **556**, 149821.

Zhao Q., Yao J., Shi L. & Wang X. (2016) Effect of calcination temperature on structure, composition and properties of $S_2O_8^{2-}/ZrO_2$ and its catalytic performance for removal of trace olefins from aromatics. *RSC Advances*, **6**, 84553–84561.

Zheng R., Porosoff M.D., Weiner J.L., Lu S., Zhu Y. & Chen J.G. (2012) Controlling hydrogenation of C=C and C=O bonds in cinnamaldehyde using silica supported Co–Pt and Cu–Pt bimetallic catalysts. *Applied Catalysis A: General*, 419–420, 126–132.

Zheng Y., Wang J., Li D., Liu C., Lu Y., Lin X. & Zheng Z. (2021) Highly efficient catalytic pyrolysis of biomass vapors upgraded into jet fuel range hydrocarbon-rich bio-oil over a bimetallic $Pt–Ni/\gamma\text{-}Al_2O_3$ catalyst. *International Journal of Hydrogen Energy*, **46**, 27922–27940.

Zhu Y., Yang M., Zhang Z., An Z., Zhang J., Shu X. & He J. (2021) NiCu bimetallic catalysts derived from layered double hydroxides for hydroconversion of *n*-heptane. *Chinese Chemical Letters*, **33**, 2069–2072.

Zhuang Y., Currie R., McAuley K.B. & Simakov D.S.A. (2019) Highly-selective CO_2 conversion *via* reverse water gas shift reaction over the 0.5 wt% Ru-promoted $Cu/ZnO/Al_2O_3$ catalyst. *Applied Catalysis A: General*, **575**, 74–86.

https://doi.org/10.1180/clm.2022.23 Published online by Cambridge University Press